AD-A147 883 A LOW-SIDELOBE SPACE FEED LENS(U) ROME AIR DEVELOPMENT 1/1
CENTER GRIFFISS AFB NY D T MCGRATH MAY 84
RADC-TR-84-116

UNCLASSIFIED F/G 9/5 NL

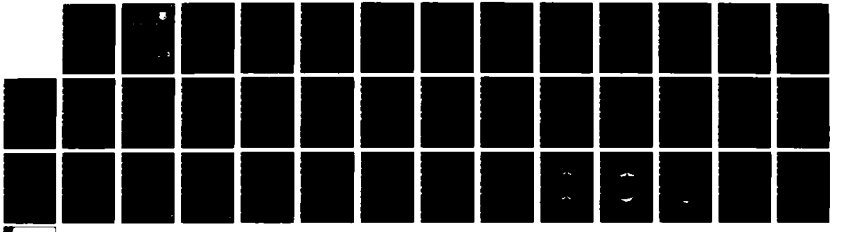

END

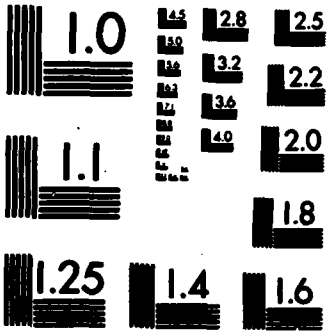

RADC-TR-84-116
In-House Report
May 1984

A LOW-SIDELOBE SPACE FEED LENS

Daniel T. McGrath, Captain, USAF

ROME AIR DEVELOPMENT CENTER
Air Force Systems Command
Griffiss Air Force Base, NY 13441

This report has been reviewed by the RADC Public Affairs Office (PA) and is releasable to the National Technical Information Service (NTIS). At NTIS it will be releasable to the general public, including foreign nations.

RADC-TR-84-116 has been reviewed and is approved for publication.

APPROVED: John K. Schindler

JOHN K. SCHINDLER, Chief
Antennas & RF Components Branch
Electromagnetic Sciences Division

APPROVED: Allan C. Schell

ALLAN C. SCHELL
Chief, Electromagnetic Sciences Division

FOR THE COMMANDER: John A. Ritz

JOHN A. RITZ
Acting Chief, Plans Office

If your address has changed or if you wish to be removed from the RADC mailing list, or if the addressee is no longer employed by your organization, please notify RADC (EEAA), Hanscom AFB MA 01731. This will assist us in maintaining a current mailing list.

Do not return copies of this report unless contractual obligations or notices on a specific document requires that it be returned.

Unclassified

SECURITY CLASSIFICATION OF THIS PAGE

REPORT DOCUMENTATION PAGE

1a. REPORT SECURITY CLASSIFICATION: Unclassified	1b. RESTRICTIVE MARKINGS
2a. SECURITY CLASSIFICATION AUTHORITY	3. DISTRIBUTION/AVAILABILITY OF REPORT: Approved for public release; distribution unlimited.
2b. DECLASSIFICATION/DOWNGRADING SCHEDULE	
4. PERFORMING ORGANIZATION REPORT NUMBER(S): RADC-TR-84-116	5. MONITORING ORGANIZATION REPORT NUMBER(S)
6a. NAME OF PERFORMING ORGANIZATION: Rome Air Development Center; 6b. OFFICE SYMBOL (If applicable): (EEA)	7a. NAME OF MONITORING ORGANIZATION
6c. ADDRESS (City, State and ZIP Code): Hanscom AFB Massachusetts 01731	7b. ADDRESS (City, State and ZIP Code)
8a. NAME OF FUNDING/SPONSORING ORGANIZATION; 8b. OFFICE SYMBOL (If applicable): (EEA)	9. PROCUREMENT INSTRUMENT IDENTIFICATION NUMBER
8c. ADDRESS (City, State and ZIP Code)	10. SOURCE OF FUNDING NOS.

PROGRAM ELEMENT NO.	PROJECT NO.	TASK NO.	WORK UNIT NO.
62702F	4600	14	01

11. TITLE (Include Security Classification): A Low-Sidelobe Space Feed Lens

12. PERSONAL AUTHOR(S): Daniel T. McGrath, Capt, USAF

13a. TYPE OF REPORT	13b. TIME COVERED	14. DATE OF REPORT (Yr., Mo., Day)	15. PAGE COUNT
In-House	FROM _____ TO _____	1984 May	40

16. SUPPLEMENTARY NOTATION

17. COSATI CODES			18. SUBJECT TERMS (Continue on reverse if necessary and identify by block number)
FIELD	GROUP	SUB. GR.	Phased array antennas; Microwave lens; Overlapped subarray antenna; Radiation patterns; Radar; (Contd)

19. ABSTRACT (Continue on reverse if necessary and identify by block number)

A parallel-plate waveguide microwave lens, constructed as part of the concept development of completely overlapped subarray antennas, was modified and tested. The lens' function is comparable to that of a Rotman lens with 16 inputs (beam ports) and 60 outputs (antenna ports). However, the input face is linear with uniformly spaced monopole elements, and the output face is circular, with monopole elements spaced uniformly in angle.

Using a four-way power divider at the center four inputs and the outputs connected to a line-source array, low sidelobe patterns were measured over a 22 percent bandwidth. Over the same 8.0 to 10.0 GHz band, total power loss in the lens was between 0.3 and 1.3 dB including mismatch, spillover and reflection losses.

Achieving those results required two major modifications to the antenna: (1) First, although image theory predicts the phase center of a ground plane-backed monopole is at the ground-plane, measurements show that when placed in an array, the phase center

20. DISTRIBUTION/AVAILABILITY OF ABSTRACT	21. ABSTRACT SECURITY CLASSIFICATION	
UNCLASSIFIED/UNLIMITED ☐ SAME AS RPT. ☐ DTIC USERS ☐	Unclassified	
22a. NAME OF RESPONSIBLE INDIVIDUAL: Daniel T. McGrath, Capt, USAF	22b. TELEPHONE NUMBER (Include Area Code)	22c. OFFICE SYMBOL: (EEA)

DD FORM 1473, 83 APR EDITION OF 1 JAN 73 IS OBSOLETE.

SECURITY CLASSIFICATION OF THIS PAGE

18. (Contd)

Bandwidth
Array antenna

---

19. (Contd)

is closer to the monopole. Its exact location depends on the element spacing in wavelengths, and will therefore change with frequency. The focal array was moved farther from the circular lens face to give good focusing at the center frequency. Second, the mismatch and coupling properties of unequally spaced elements along the circular face varied enough to distort the amplitude taper, causing higher sidelobes. An optimum uniform spacing eliminated that problem, and it is shown that it is possible, in general, to find such a spacing that will not degrade the lens' performance either as a beam-former or as a transform feed.

Preface

First and foremost the author thanks Major Hugh L. Southall who oversaw the design and fabrication of this antenna and graciously passed on his knowledge and experience. Thanks also to the personnel of RADC's Ipswich Site, in particular Mr. Edward Martin, for his conscientious performance of often tedious measurements, and to Mr. Raymond Schofield for his precise, professional machine work.

Contents

1.	INTRODUCTION	7
	1.1 The Completely Overlapped Subarray Concept	8
	1.2 Array Lens Original Design	11
2.	MODIFICATIONS	14
	2.1 Phase Center Correction	14
	2.2 Uniform Element Spacing	17
3.	PERFORMANCE RESULTS	18
	3.1 Phase Linearity and Phase Center	18
	3.2 Element Mismatch	22
	3.3 Efficiency	23
	3.4 Antenna Patterns	24
4.	CONCLUSIONS	25
GLOSSARY		27
REFERENCES		29
APPENDIX A:	Minimization of Phase Error for Uniform Spacing of Cylindrical Lens Elements	31

Illustrations

1.	Completely Overlapped Subarray Antenna	9
2.	Subarray Beams	10
3.	Lens Coordinate Convention	12
4.	Lens Original Design	13
5.	Array Lens Phase Response, 1LB Active, 9 GHz, Original Lens	15
6.	Far Field Pattern of 1LB, 9 GHz, Original Lens	16
7.	Theoretical Monopole Element Patterns	16
8.	VSWR and Mismatch Loss of Face C Elements, 9 GHz, Original Lens	17
9.	Array Lens Phase Response, 1LB Active, 9 GHz, Modified Lens	19
10.	Far Field Pattern of 1 LB, 9 GHz, Modified Lens	20
11.	Array Lens Phase Response, 1LB Active, 8 GHz, Modified Lens	21
12.	Apparent Phase Center Location vs Frequency	21
13.	VSWR of Face C Elements, Modified Lens	22
14.	Measured Antenna Pattern, 8.25 GHz	24
15.	Measured Antenna Pattern, 9 GHz	25
16.	Measured Antenna Pattern, 9.75 GHz	26
A1.	Aperture Distribution of Subarray Beam No. 7	32
A2.	Distorted Aperture Distribution of Subarray Beam No. 7	33
A3.	Total Aperture Amplitude Distribution	34
A4.	Total Aperture Phase Distribution	34
A5.	Theoretical Antenna Patterns	37
A6.	Strength of First Sidelobe vs Probe Spacing	40
A7.	Peak Sidelobe Level vs Scan Angle and Frequency	40

Tables

1.	Performance Parameters, COSA Array Lens	8
2.	Element Excitation Amplitude and Phase	23

A Low-Sidelobe Space Feed Lens

1. INTRODUCTION

A parallel plate waveguide feed lens for a 60-element linear array was built and tested as part of the concept verification of the completely overlapped subarray antenna (COSA) concept.[1, 2] The technique uses two microwave lenses in series to achieve high instantaneous bandwidth in a low-sidelobe antenna. However, the properties of the single array lens in bandwidth, low phase error and high efficiency make it an alternative to waveguide or coax feeds for linear and planar phased array antennas.

This report will discuss the COSA concept briefly, as an explanation of the original lens design. The modifications to that design will be described in detail, as well as the measurements that were made to demonstrate its performance. In particular, the phase centers of the monopole elements were found to be elsewhere than predicted, requiring repositioning of the focal array. Second, the mismatch and coupling properties of unequally spaced elements along the circular lens face varied enough to distort the amplitude taper, causing higher sidelobes. An optimum uniform spacing eliminated that problem.

(Received for publication 4 June 1984)

1. Fante, R. L. (1979) Study of the Radiation Properties of Overlapped, Subarrayed Scanning Antennas, RADC-TR-82-32, AD A082401.

2. Southall, H. L. (1980) Completely-overlapped-subarray fed antenna for broadband, wide scan angle, low sidelobe radar applications, Proceedings 1980 Antenna Applications Symposium, Monticello, Illinois.

With these improvements, the lens performed comparably to a printed circuit Rotman lens. Table 1 summarizes the results achieved.

Table 1. Performance Paramaters, COSA Array Lens

Sidelobe Level	Peak rms	-32 dB -39 dB
Bandwidth	Tunable Instantaneous	22% 7.4% at 55° Scan
Amplitude Error	9 GHz	0.3 dB rms
Phase Error	9 GHz	3° rms
Insertion Loss	9 GHz Average	1.3 dB 0.8 dB

1.1 The Completely Overlapped Subarray Concept

The far field pattern factor of a linear array with the conventional "corporate" feed and steered with phase shifters is

$$f(\theta, \theta_o) = \sum_n a_n \exp \left\{ -j\, 2\pi\, d(n - \tfrac{1}{2}) \left(\frac{\sin\theta}{\lambda} - \frac{\sin\theta_o}{\lambda_o} \right) \right\} \qquad (1)$$

where θ is the observation angle, θ_o is the desired scan angle, d is the distance between elements, λ is the wavelength, λ_o is the wavelength at center frequency and a_n is the relative amplitude applied to the n'th element. The peak of the main beam is at the angle θ that makes the exponent in Eq. (1) equal to zero and clearly $\theta = \theta_o$ only when $\lambda = \lambda_o$. Hence for frequencies other than $f_o = c/\lambda_o$, transmitted energy is directed at some angle other than the desired θ_o and the consequence is a loss of bandwidth.

The most straightforward way to correct this problem is to replace the phase shifters with time delay units, but unfortunately conventional time delayers are either too bulky, lossy or expensive for practical use in a large planar array. Tang[3] discusses a number of alternatives, all of which involve replacing the corporate feed with some other structure, and shows that a transform feed is the optimum in terms of signal bandwidth.

3. Tang, R. (1972) Survey of time-delay beam steering techniques, in Phased Array Antennas, Ed., Oliver, A.A., and Knittel, G.H., pp. 254-260, Artech House, Dedham, Massachusetts.

The RADC implementation of the concept is Figure 1. A 60-element array of monopole probes radiates into free space from a flared aperture. Similar elements along the curved surface of a large parallel-plate waveguide connect to the aperture elements with coaxial cables, all of the same length. On the opposite face of this waveguide, or "array lens" is a 16-element monopole array which, in turn, connects (again with coaxial cables) to the "antenna port" elements of a Rotman lens. The Rotman lens is also a parallel plate waveguide, with two monopole arrays concave to each other (16 elements each plus two dummy-loaded elements). Finally, the "beam port" elements are fed by a corporate-feed power divider, which will include time-delayers. It is important to note that this concept does not obviate the need for time-delay units, but it does reduce the number required (in this case by 16/60, but for a planar array by $16^2/60^2$).

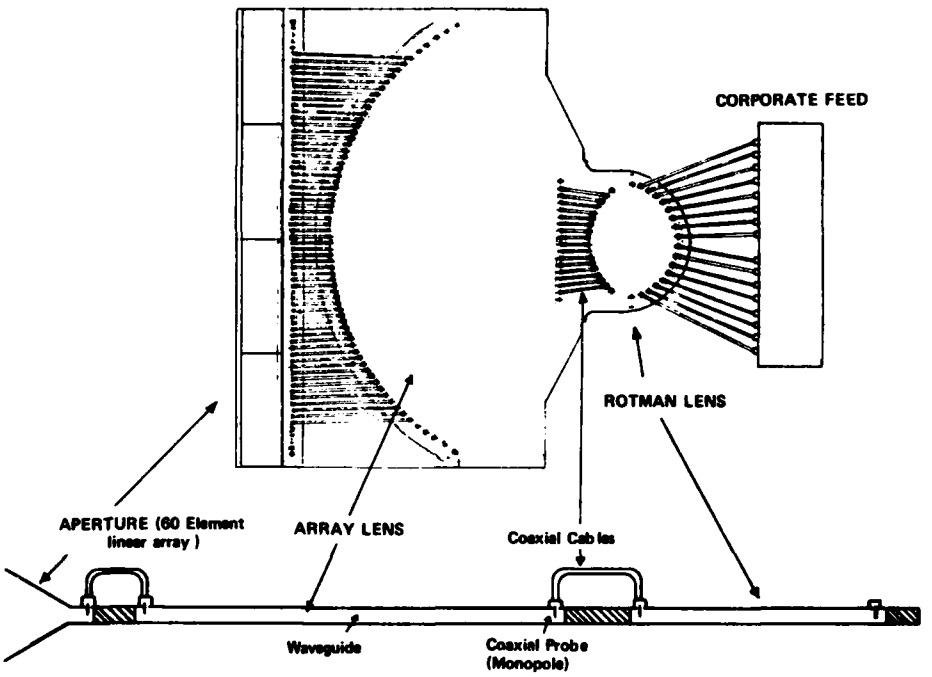

Figure 1. Completely Overlapped Subarray Antenna

If we were to drive a single beam port of the Rotman lens, the antenna port elements would be illuminated with constant amplitude and progressive phase shift

between each. Hence, the linear array in the array lens will illuminate the curved face with a sin $(8\gamma)/\sin(\gamma/2)$ beam of constant phase with $\gamma = kd \sin\theta$ (Figure 2).

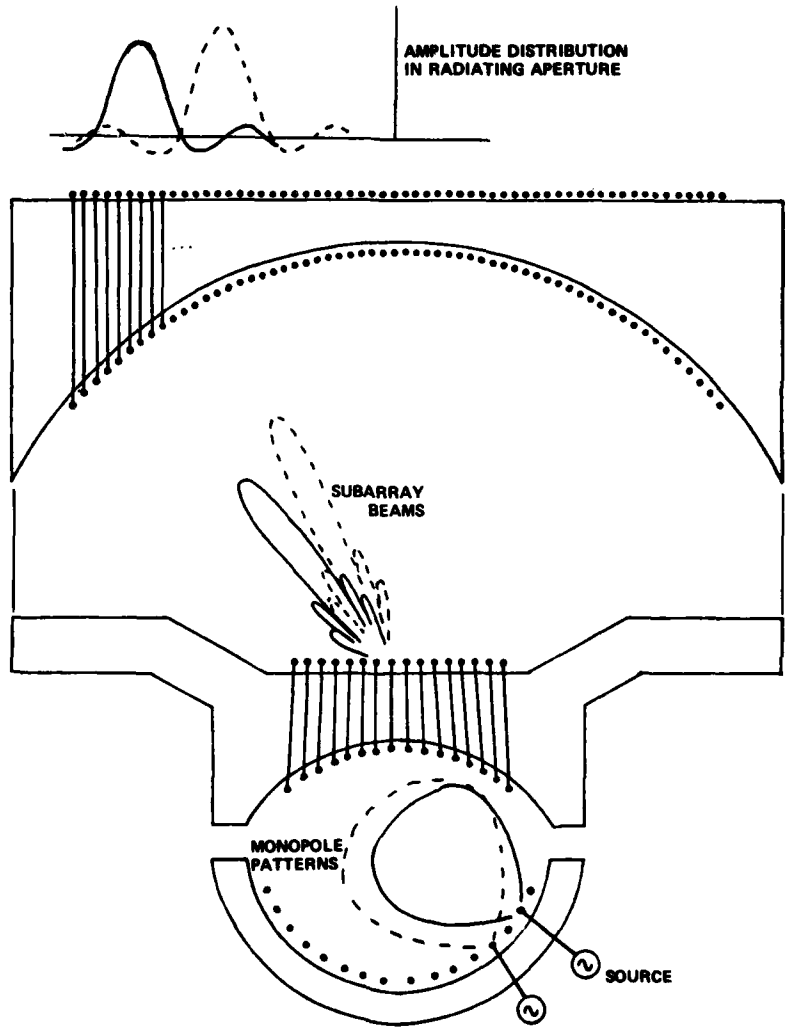

Figure 2. Subarray Beams

With all 16 beam ports driven simultaneously, these "subarray" beams add vectorially at the 60 array lens elements to produce desired phase and amplitude distributions a_n and α_n respectively. The pattern produced by the aperture array is then:

$$f(\theta, \theta_o) = \sum_n a_n \exp \left\{ -j \left[2\pi d(n - \tfrac{1}{2}) \left(\frac{\sin\theta}{\lambda} - \frac{\sin\theta_o}{\lambda_o} \right) + \alpha_n \right] \right\} . \quad (2)$$

If

$$\alpha_n = -2\pi d(n - \tfrac{1}{2}) \left(\frac{\sin\theta_o}{\lambda} - \frac{\sin\theta_o}{\lambda_o} \right) \quad (3)$$

then Eq. (2) becomes

$$f(\theta, \theta_o) = \sum_n a_n \exp \left\{ -j\, 2\pi \frac{d}{\lambda} (n - \tfrac{1}{2}) (\sin\theta - \sin\theta_o) \right\} \quad (4)$$

for which the main beam is directed at $\theta = \theta_o$ for any λ. We know the angle at which each subarray beam points inside the array lens, and hence which of the 60 elements its peak illuminates. Then to produce the desired α_n a time delay of

$$\tau = 2\pi d(n - \tfrac{1}{2}) \frac{\sin\theta_o}{\lambda} \quad (5)$$

and a phase shift

$$\psi = 2\pi d(n - \tfrac{1}{2}) \frac{\sin\theta_o}{\lambda_o} \quad (6)$$

are applied at that beam port, using switched line lengths for time delay. In short, the correct phase-amplitude distribution at the aperture is expanded in the "sinc" functions produced by the subarray beams. For the technique to work, each of the two lenses must perform a (spatial) discrete Fourier transformation (DFT).

1.2 Array Lens Original Design

That DFT requirement dictates the structure of the array lens. Using the coordinate convention shown in Figure 3, the path length from any point x_n, y_n on the curved face (face C) to any point x_m, y_m on the flat face is

$$R_{mn} = \left\{ (x_n - x_m)^2 + (y_n - y_m)^2 \right\}^{1/2} \quad (7)$$

since $F^2 = x_n^2 + y_n^2$, and $y_m = 0$

$$R_{mn} = \left\{ F^2 + x_m^2 - 2\, x_n x_m \right\}^{1/2} \quad (8)$$

and using the binomial approximation

$$R_{mn} \approx F + \frac{x_m^2}{2F} - \frac{x_n x_m}{F} . \tag{9}$$

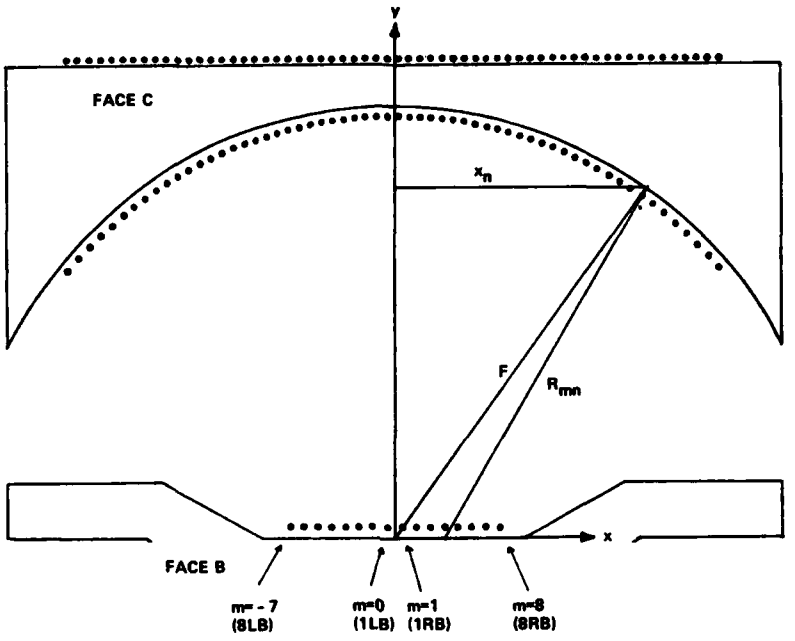

Figure 3. Lens Coordinate Convention

The quadratic term $x_m^2/2F$ is removed by adding cable lengths of $\ell_o - x_m^2/2F$ at face B, where ℓ_o is an arbitrary constant. The voltage at element n can be expressed as a sum of contributions from each element m:

$$V_n = \sum_m \frac{e^{jk R_{mn}}}{\sqrt{R_{mn}}} \tag{10}$$

$$\approx \frac{e^{j 2\pi F/\lambda}}{\sqrt{F}} \sum_m V_m e^{-j\frac{2\pi}{\lambda F} x_m x_n} \tag{11}$$

where Eq. (10) uses the Green's function for propagation between parallel plates $E(r) = e^{jkr}/\sqrt{r}$ and next assumes that for any n, $R_{mn} \approx F$ for all m. Under the condition that the elements on both faces are uniformly spaced in x (by distance d at face C and δ at face B):

$$V_n = C_o \sum_m V_n e^{-j\frac{2\pi\delta d}{\lambda F}(n-\frac{1}{2})(m-\frac{1}{2})} \qquad (12)$$

which is the desired form of DFT in the lateral direction, x. The spacing, d, of face C elements in the x direction was chosen as $\lambda_o/2$, the same as the 60-element linear array. Lens focal length, F and face B element spacing δ were chosen to yield 20 percent bandwidth at 55° scan (fractional bandwidth depends on the size of the array at face B and on F, Reference 1). Assuming that image theory applied to the ground-plane-backed monopole, the radius of the face C arc was chosen as F and the ground-plane of face B was located on the lens diameter. Elements at both faces were placed 0.39 λ_o from the ground-plane, using experimental results of White et al.[4] The resulting lens design is shown in Figure 4.

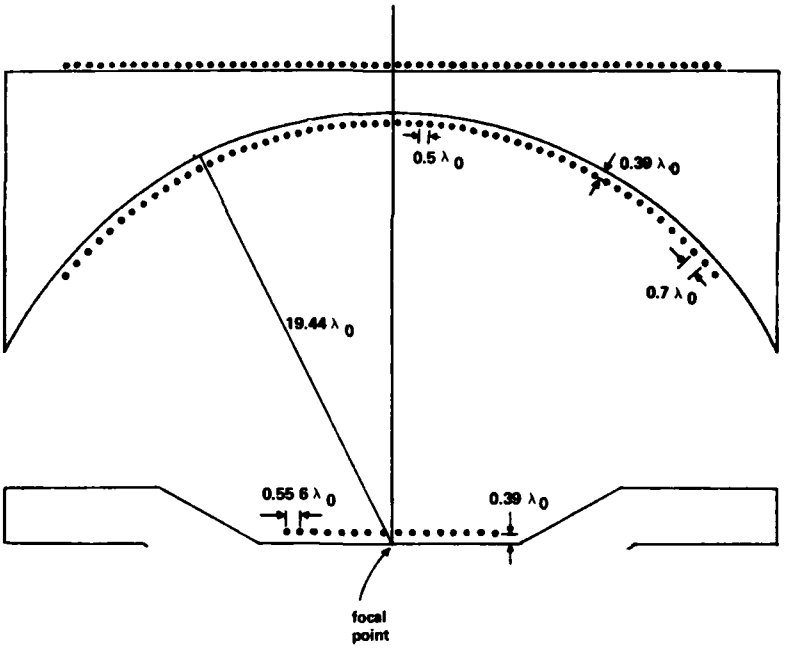

Figure 4. Lens Original Design

4. White, Z.O., Wong, W., and Southall, H.L. (1982) Probe Element Matching in a Parallel-Plate Waveguide Array, RADC-TR-82-163, AD A120865.

2. MODIFICATIONS

Two major modifications to the array lens were necessary: First, it was discovered that the monopole elements did not behave as predicted by image theory—that is, they appear to radiate not from the vertical ground-plane behind the array, but from some point closer to the monopole; and second, because elements along the circular face were not evenly spaced, it was impossible to match them to the same VSWR. Hence, there was a mismatch loss that was low on the outside and high on the inside, which distorted the low-sidelobe amplitude taper. To correct these effects, the linear array was moved slightly farther away from the curved face so that the monopoles, rather than their image plane, are on the focal plane; and the curved face was re-machined to space those elements uniformly.

2.1 Phase Center Correction

In a simplified analysis, considering the monopole as a point source at a distance g from an infinite ground-plane, the radiated field, by image theory, should be that of two sources separated by distance 2g and driven 180° out of phase.[5] A locus of constant phase is then a circle around the normal projection of the element onto the ground-plane. This was the rationale for placing the ground plane of the flat lens surface on the diameter of the circular face.

Figure 5 shows the measured phase of the "face C" ports (*HP 8408 Automatic* Network Analyzer) when a single port (No. 1L) of the linear array is transmitting and all others terminated in 50Ω. Because the active port is to one side of the lens focal point, it is not expected to illuminate the arc with constant phase, but rather an approximately linear phase progression, as indicated by the solid line. The measured data agrees better with the dashed line, which is the predicted response assuming that the phase center is at the probe itself rather than at the ground-plane behind it. For Figure 6 the face C elements were connected by coaxial cables to the aperture array, and the receiver was connected to port 1LB. Again, under the assumption that the linear array element receives a constant amplitude and linear phase from the elements of the curved array, the measured pattern should be an ideal sin $(N\gamma/\sin\gamma)$ function. However, the nulls of the pattern are filled in, which is an indication that the beam is not focused—or again, the receiving element is not in the lens' focal plane.

---

5. Harrington, R. L. (1961) Time-Harmonic Electromagnetic Fields, McGraw-Hill, New York.

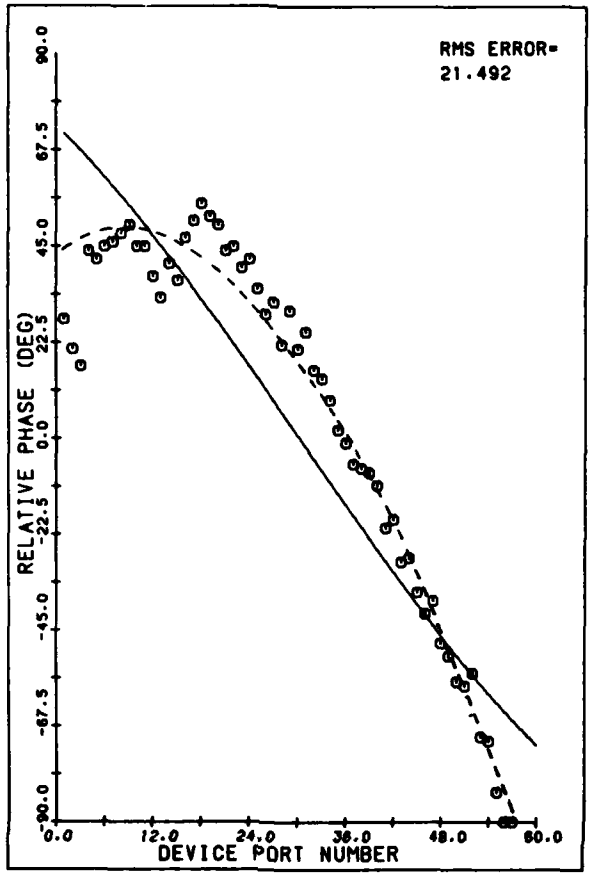

Figure 5. Array Lens Phase Response, 1LB Active, 9 GHz, Original Lens

The conclusion drawn from these measurements is that image theory does not strictly apply to elements of an array. Analysis and measurements by Tomasic[6] indicate that due to mutual coupling between monopole elements, the phase of the element pattern is not constant, but decreases rapidly near the end-fire grating lobe angle

$$\theta_{EFGL} = \sin^{-1}\left\{\frac{\lambda}{d} - 1\right\} \tag{13}$$

as shown in Figure 7. This effect will in general cause the apparent phase center to move closer to the element for spacings greater than one-half wavelength.

6. Tomasic, B., and Hessel, A. (1982) Linear phased arrays of coaxially-fed monopole elements in a parallel plate guide, in 1982 APS Symposium Digest, pp. 144-147.

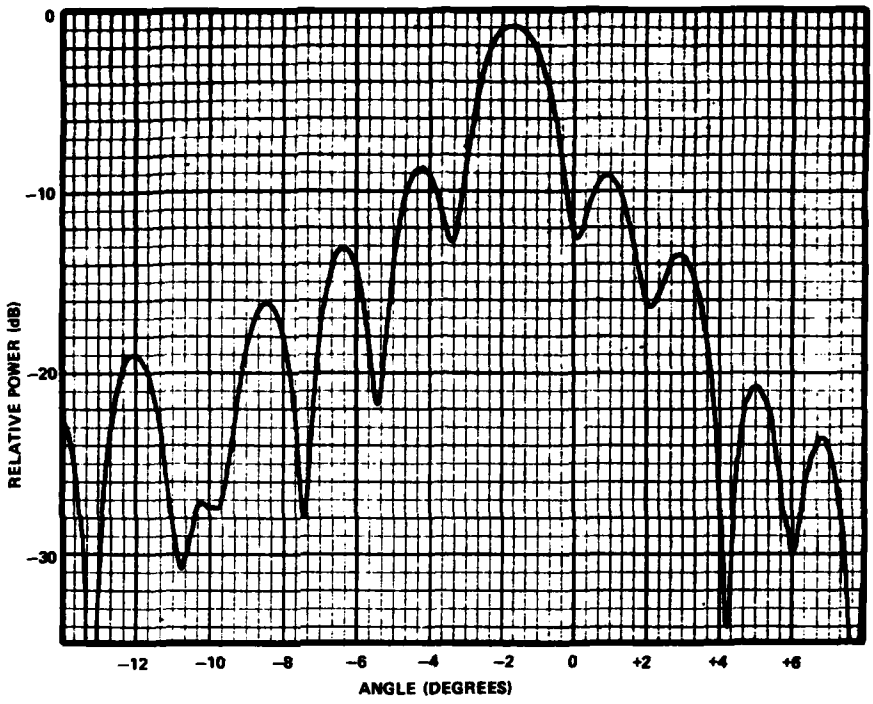

Figure 6. Far Field Pattern of 1LB, 9 GHz, Original Lens

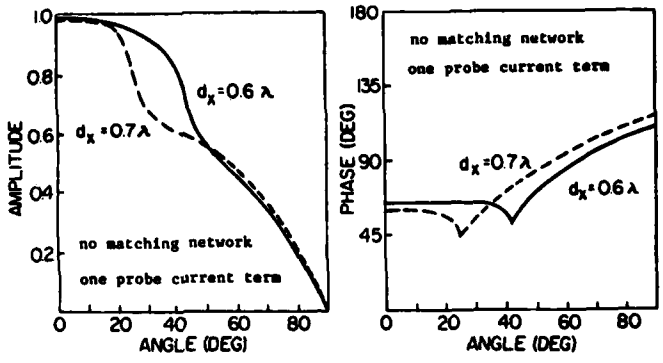

Figure 7. Theoretical Monopole Element Patterns
(Courtesy of B. Tomasie)

2.2 Uniform Element Spacing

Not only are the pattern nulls of Figure 2 filled in, but the sidelobes are much higher than the 13 dB expected. Yet, considering the element pattern of the receiving probe inside the lens, which naturally applies a (slight) taper, one expects the sidelobes would be lower, not higher. This discrepancy is the consequence of the uneven spacing of elements along the curved face—they are spaced evenly in the lateral direction, hence quadratically along the arc. The VSWR is quite sensitive to spacing between elements, and hence varies from probe to probe. Figure 8 shows the measured VSWR and calculated mismatch loss of the 60 elements. Because the mismatch is worse in the center, there is a natural "inverse" taper applied to the array, which raises the sidelobes.

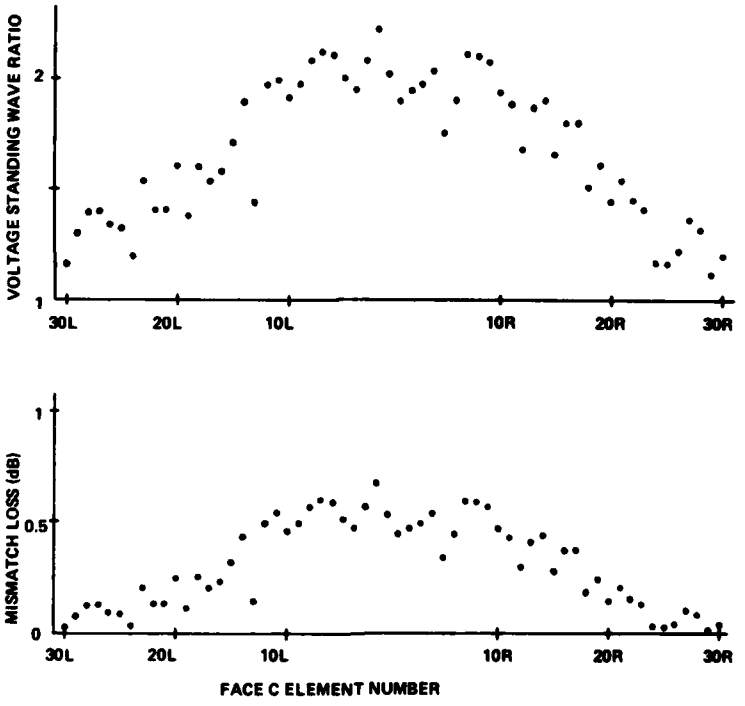

Figure 8. VSWR and Mismatch Loss of Face C Elements, 9 GHz, Original Lens

It is possible to adjust the probe length and ground-plane spacing to achieve a better match, and conceivably by making those parameters variable from element

to element, to get the same low VSWR on all elements. However, there is phase delay between the incident field in the coaxial aperture and the radiated field in the waveguide, which must also vary with ground-plane spacing and probe length. If the two parameters are not the same for all elements, the phase will not be linear, that is, a varying insertion phase would replace the varying insertion loss. The best solution, in this case, is to make all the array elements the same, spaced at equal intervals in angle along the curved face. The problem is doing so, as explained in Appendix A, is that when a time delay steering term is introduced at the Rotman lens inputs there will be a distortion of the phase gradient at the aperture array because its elements are no longer at the same lateral position as those inside the lens. For this antenna, the optimum spacing is 1.55°, but, in general, it will depend on focal length F and aperture width L. The criteria used in finding the correct spacing were minimum rms phase error and zero average phase error. Because the average error is zero there is no squint with frequency and hence no degradation of bandwidth. Just as the aperture phase is slightly "warped" by this modification, so is the amplitude. However, the new amplitude distribution actually yields lower peak sidelobes in the error-free pattern (-50 dB vs -35 dB in the original design).

Note that the phase center problem does not affect the elements of the circular face because they are all oriented approximately broadside to face B. However, the chosen ground plane spacing of 0.39 λ_o, although acceptable in terms of VSWR, yields an element pattern with peaks near ± 45° and -5 dB at broadside. Along with the other modifications, this was reduced to 0.20 λ_o at both faces of the array lens.

3. PERFORMANCE RESULTS

3.1 Phase Linearity and Phase Center

Aside from its function in the COSA antenna, the array lens is simply a beamformer. When a single port on either face is excited, all ports of the opposite face should, ideally, be illuminated with the same amplitude and a constant phase increment between ports. The 60-element linear array connected to those illuminated ports will then radiate a $\sin(60\gamma)/\sin(\gamma)$ beam ($\gamma = 1/2\ kd \sin\theta$). As Figures 5 and 6 showed, this was not the case, because of phase center shift and varying mismatch loss.

Figure 9 shows the measured phase, after modification, at face C when a single port of face B is excited, and is much closer to the desired result (solid line). The H-plane pattern measured with a receiver connected to this element (Figure 10) exhibits clear, sharp nulls and the -13 dB sidelobes of a "sinc" function. However,

Figure 11 shows that at 8 GHz there is a significant deviation from the predicted phase (the solid line is calculated with the phase center assumed to be at the probe) and it is in the opposite direction of the error in Figure 5. This suggests that although the phase center is very close to the probe at the center frequency of 9 GHz, it is still nearer the groundplane at 8 GHz.

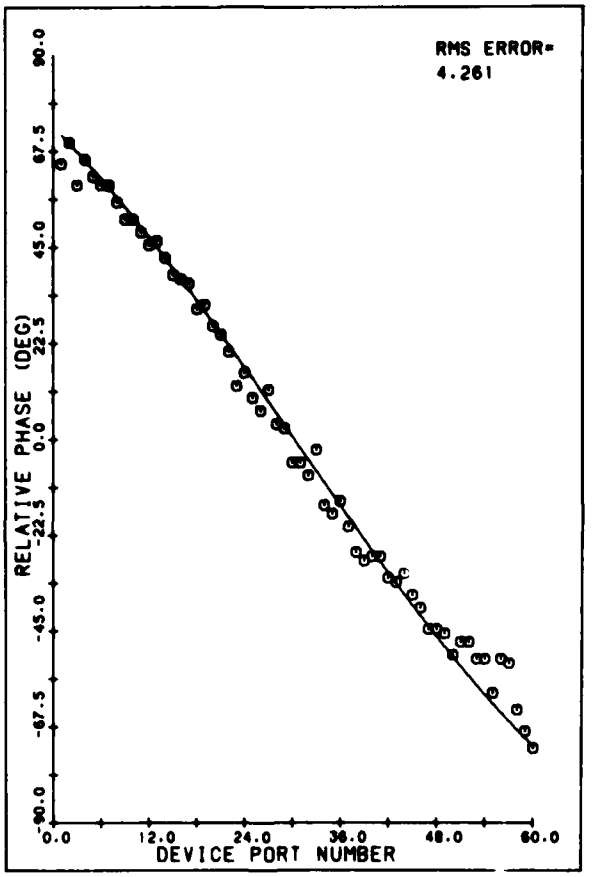

Figure 9. Array Lens Phase Response, 1LB Active, 9 GHz, Modified Lens

To attempt to isolate the phase center location better, the following procedure was used: A point source is assumed to be located at a distance g from the face B ground plane, and the phase at each port of face C due to the source is computed. The rms error between that predicted phase and the measured phase is then

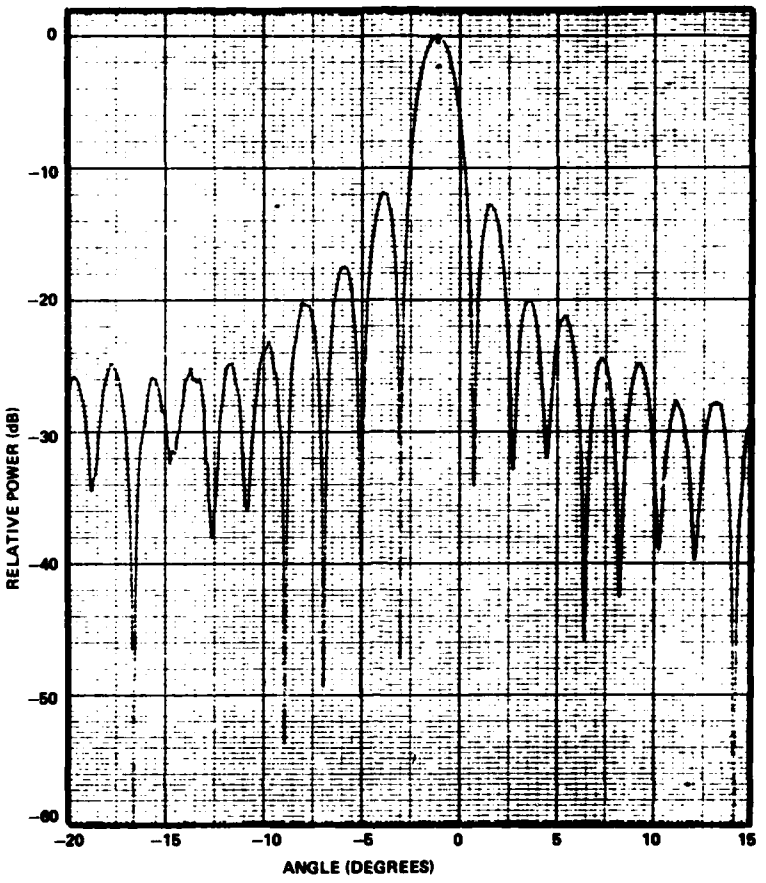

Figure 10. Far Field Pattern of 1LB, 9 GHz, Modified Lens

calculated as g is varied from zero to twice the actual probe-to-ground distance. The results, using measured data from both 1LB and 1RB at frequencies from 8 to 10 GHz, are shown in Figure 12. Below center frequency, the phase center shifts toward ground; and above f_o it shifts away from ground. Apparently, the exact location depends on the spacing between elements in wavelengths which, of course varies with frequency.

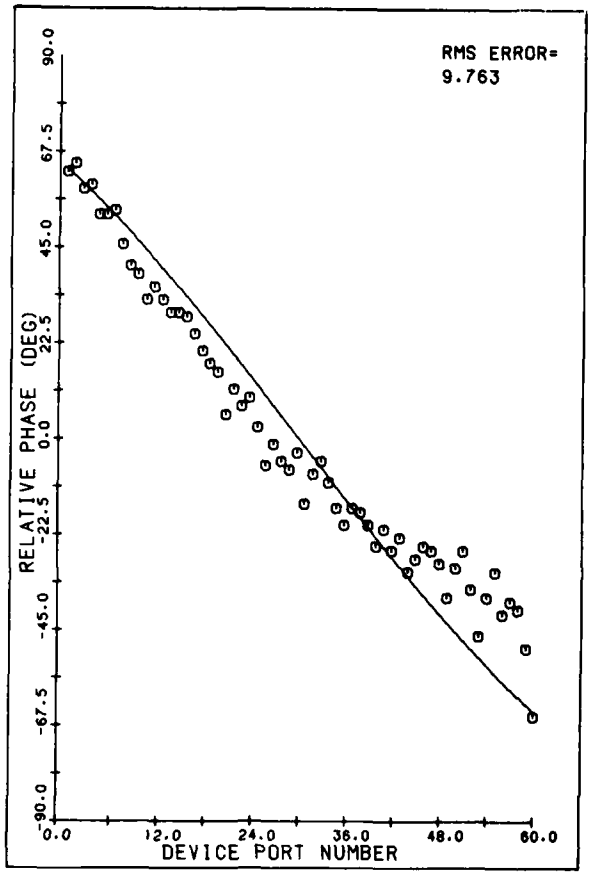

Figure 11. Array Lens Phase Response 1LB Active, 8 GHz, Modified Lens

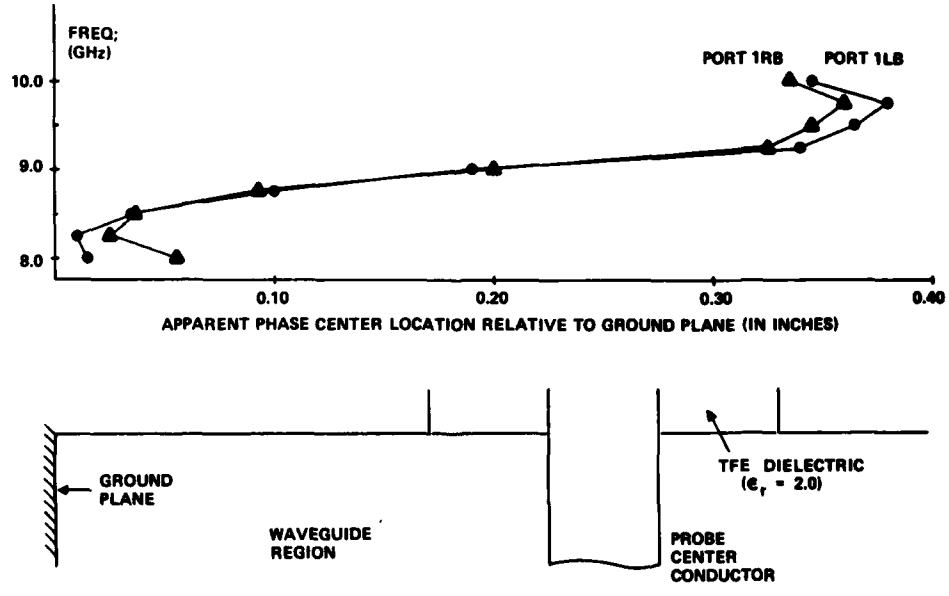

Figure 12. Apparent Phase Center Location vs Frequency

3.2 Element Mismatch

Figure 13a shows the measured VSWR of the face C elements after modification, and Figure 13b is the VSWR vs frequency of a few typical elements. Clearly, the uniform spacing accomplished the desired result: all elements see essentially the same environment and are well-matched over a wide frequency range. The principal effect of this change is in the lower sidelobes of Figure 10.

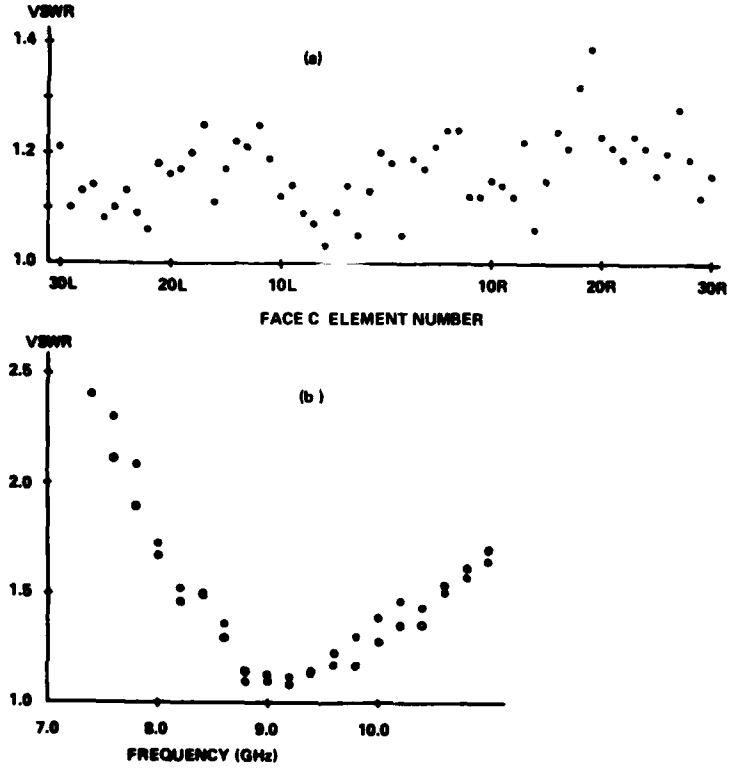

Figure 13. VSWR of Face C Elements, Modified Lens

The response of these monopole elements is very sensitive to length ℓ, element spacing d, and ground plane spacing g. The parameters that we have found to give lowest VSWR at 9 GHz are given below. There is some question, however, whether these are optimum in terms of efficiency—power can be lost through coupling to other elements as well as mismatch, and the lowest VSWR does not necessarily imply greatest radiated power.

Circular Face	Linear Face
ℓ = 0.280" = 0.213 λ_o	ℓ = 0.270" = 0.206 λ_o
d = 0.683" = 0.520 λ_o	d = 0.730" = 0.556 λ_o
g = 0.262" = 0.20 λ_o	g = 0.262" = 0.20 λ^o
waveguide height	= 0.40" = 0.305 λ_o
probe radius, center conductor	= 0.025"
probe radius, dielectric	= 0.081"

3.3 Efficiency

For the lens to produce a low-sidelobe pattern, four or more ports of the linear face are driven simultaneously. For these measurements, the excitations shown in Table 2 were used. This is simply the ideal response of the center four Rotman lens antenna ports when the beam ports are driven in phase with a cosine-pedestal amplitude taper. The lens insertion loss is calculated as $IL_{dB} = 10 \log_{10}$ (Total Power Out/Total Power In)

$$= 10 \log_{10} \left\{ \sum_n 10^{-IL_n/10} \Big/ \sum_p 10^{-IL_r/10} \right\} \qquad (14)$$

where IL_n is the measured loss in dB at each of the 60 ports of the cylindrical face and IL_p is the measured loss at the four power divider ports. The results shown below for the nine frequencies measured average to 0.84 dB.

Frequency (GHz)	8.0	8.25	8.5	8.75	9.0	9.25	9.5	9.75	10.0
Ins. Loss (dB)	0.3	0.4	0.3	0.7	1.3	1.3	1.3	1.2	1.2

Table 2. Element Excitation Amplitude and Phase

Port	Amplitude (dB)	Phase (Deg)
2L	-10	+6
1L	0	0
1R	0	0
2R	-10	+6

3.4 Antenna Patterns

Using the four-way power divider described above connected to the four central ports of face B, the scientific Atlanta 2020 System was used to measure the antenna patterns. Figures 14, 15 and 16 are representative results, at 8.25, 9.0 and 9.75 GHz. These measurements show that low sidelobe performance was achieved over the entire 20 percent bandwidth. At center frequency the highest sidelobe is -32 dB which is comparable to results reported by Maybell[7] who used a printed circuit Rotman lens with six weighted beam ports.

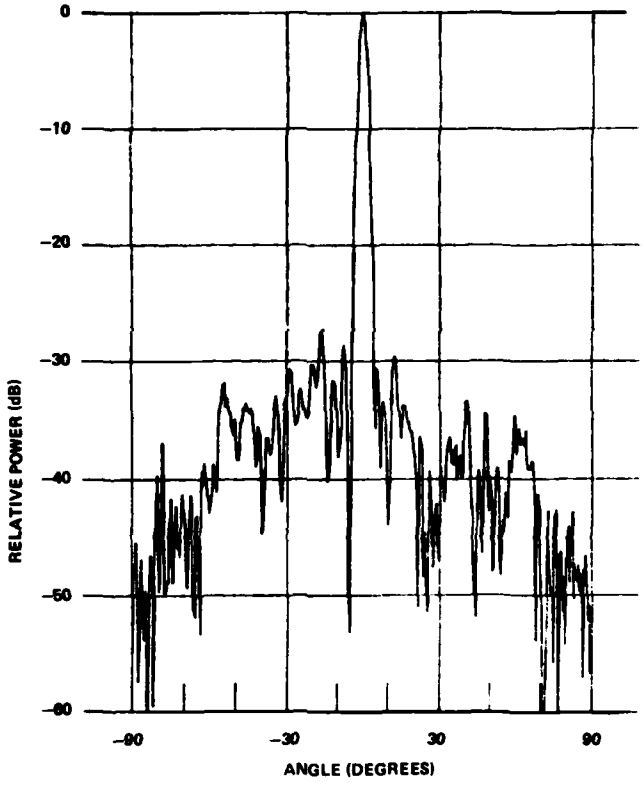

Figure 14. Measured Antenna Pattern, 8.25 GHz

7. Maybell, M. J. (1983) Printed Rotman lens - fed array having wide bandwidth, low sidelobes, constant beamwidth and synthesized radiation pattern, in 1983 APS Symposium Digest, pp. 373-376.

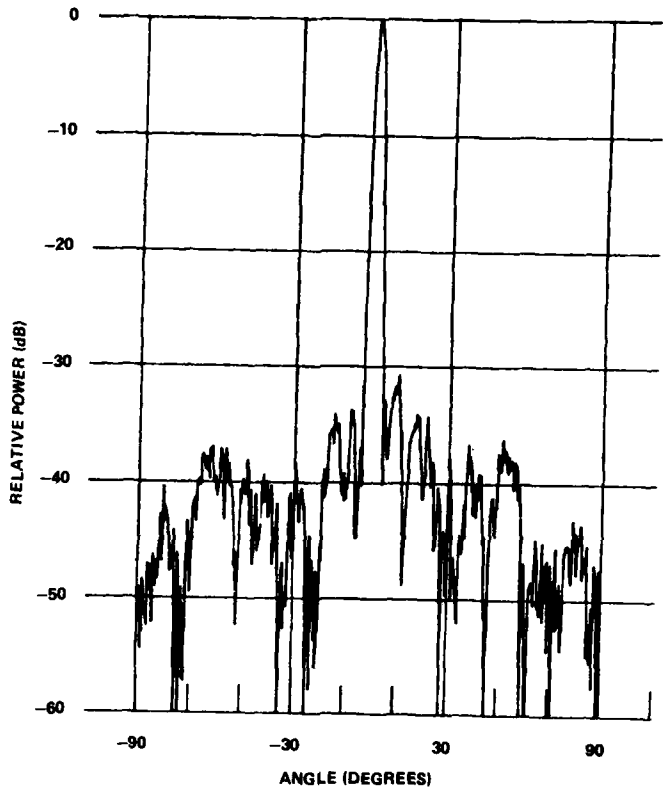

Figure 15. Measured Antenna Pattern, 9 GHz

4. CONCLUSIONS

We have achieved low-sidelobe performance over a wide bandwidth with a parallel-plate waveguide lens. Two major changes to the original design were necessary: First, we repositioned the beam port array to place the monopole elements' phase centers in the lens focal plane. The exact location of that phase center depends on element spacing in wavelengths and thus varies with frequency. Second, we relocated the elements along the circular face for uniform spacing, and hence uniform low VSWR match anduniform mutual coupling. This change will cause some degradiation in the lens' function as a transform feed, but only at the very limit of both frequency and scan angle.

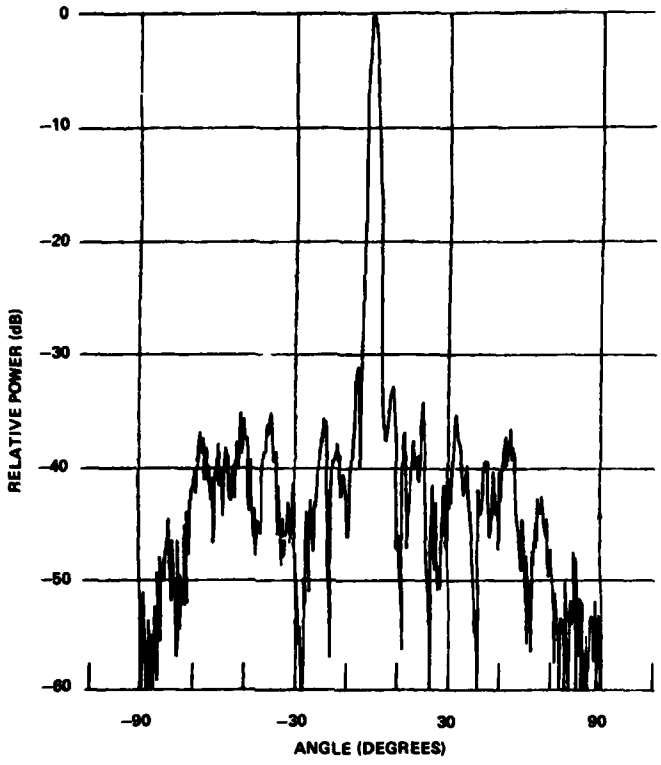

Figure 16. Measured Antenna Pattern, 9.75 GHz

Others have achieved comparable sidelobe performance with printed circuit Rotman lenses. This waveguide lens has the advantages of greater efficiency and higher power-handling capability. Its relative simplicity of design makes fabrication easier than for a waveguide Rotman lens, which has two curved faces with non-uniform element spacings on both.

However, the completely overlapped subarray antenna must use a Rotman lens as well as the array lens discussed in this report. The performance of the latter is clearly adequate and the next step in this ongoing project must be to find an improved parallel-plate Rotman lens design.

Glossary

α_n - Time delay phase correction

M - Number of elements in the linear array of the lens (16)

N - Number of aperture elements (60)

m - Index of face B elements

n - Index of face C elements

d - Spacing of face C elements

δ - Spacing of face B elements

λ - Wavelength

λ_o - Wavelength at center frequency (9.0 GHz)

θ_o - Scan angle from aperture broadside

ℓ - Aperture length

F - Lens radius, or focal length

k - Wavenumber $k = 2\pi/\lambda$

face A - Beam port side of the Rotman lens

face B - Array lens flat face and Rotman lens antenna ports

face C - Array lens circular face and aperture array

References

1. Fante, R. L. (1982) Study of the Radiation Properties of Overlapped, Subarrayed Scanning Antennas, RADC-TR-82-32, AD A082401.
2. Southall, H. L. (1980) Completely-overlapped-subarray fed antenna for broad-band, wide scan angle, low sidelobe radar applications, Proceedings 1980 Antenna Applications Symposium, Monticello, Illinois.
3. Tang, R. (1972) Survey of time-delay beam steering techniques, in Phased Array Antennas, Ed., Oliver, A. A. and Knittel, G. H., pp. 254-260, Artech House, Dedham, Massachusetts.
4. White, Z. O., Wong, W., and Southall, H. L. (1982) Probe Element Matching in a Parallel-Plate Waveguide Array, RADC-TR-82-163, AD A120865.
5. Harrington, R. L. (1961) Time-Harmonic Electromagnetic Fields, McGraw-Hill, New York.
6. Tomasic, B., and Hessel, A. (1982) Linear phased array of coaxially-fed monopole elements in a parallel plate guide, in 1982 APS Symposium Digest, pp. 144-147.
7. Maybell, M. J. (1983) Printed Rotman lens - fed array having wide bandwidth, low sidelobes, constant beamwidth and synthesized radiation pattern, in 1983 APS Symposium Digest, pp. 373-376.

Appendix A

Minimization of Phase Error for Uniform Spacing of Cylindrical Lens Elements

The array factor for a phase shifter-steered linear array of N elements is

$$f(\theta, \theta_o) = \sum_{n=1-\frac{N}{2}}^{\frac{N}{2}} a_n \exp\left\{-j\,2\pi\, d\,(n-\tfrac{1}{2}) \quad \left(\frac{\sin\theta}{\lambda} - \frac{\sin\theta_o}{\lambda_o}\right)\right\} \qquad (A1)$$

where d is the spacing between elements in units of length, λ_o is the wavelength at center frequency, θ_o is the desired scan angle and a_n is the amplitude applied to each element. The instantaneous bandwidth of the array is limited by the fact that for $\lambda \neq \lambda_o$ the beam peak is at some angle $\theta \neq \theta_o$. The completely overlapped subarray feed applies a frequency-dependent phase correction at the phase shifter inputs:

$$\alpha_n = d(n-\tfrac{1}{2}) \sin\theta_o \left(\frac{1}{\lambda} - \frac{1}{\lambda_o}\right) \qquad (A2)$$

so that the pattern factor is

$$f(\theta, \theta_o) = \sum_n a_n \exp \left\{-j\, 2\pi\, d(n-\tfrac{1}{2}) \left(\frac{\sin\theta}{\lambda} - \frac{\sin\theta_o}{\lambda_o}\right) + j\, 2\pi\, \alpha_n\right\}$$

$$= \sum_n a_n \exp \left\{-j\, \frac{2\pi\, d}{\lambda}(n-\tfrac{1}{2})\, (\sin\theta - \sin\theta_o)\right\} \qquad \text{(A3)}$$

which is maximum for $\theta = \theta_o$ for all λ.

In the case of a COSA (completely overlapped subarray antenna) this correction term is formed by vector addition of time delayed sin $(M\gamma)$/sin (γ) beams produced by the Rotman lens and illuminating the cylindrical face of the array lens. This sum of the individual subarray beams should be a tapered amplitude distribution with a linear phase tilt corresponding to the desired squint correction, α_n.

Consider subarray beam No. 7, directed at $\theta = 37.8°$ from the face B normal. Assuming that the cylindrical face (face C) is in the far field, the 16-element linear array produces the amplitude shown in Figure A1, with constant phase.

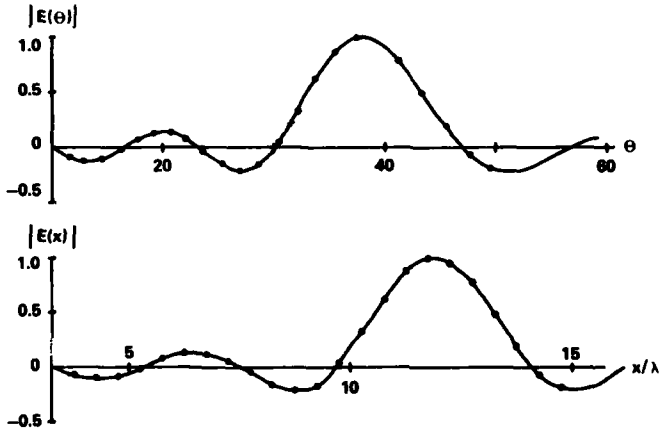

Figure A1. Aperture Distribution of Subarray Beam No. 7

Note that it appears skewed when plotted vs θ because it is sin$(M\gamma)$/sin(γ), $\gamma = kd/2 \sin\theta$, rather than sin$(M\theta)$/sin(θ). Yet in the aperture, we want sin(Mx)/sin(x), and hence we must sample the field inside the lens at intervals of $\sin\theta = c(n - 1/2)$, with c a constant determined in the initial design (in this case $c = d/F$, where F is the lens focal length). Clearly, any uniform spacing of lens elements will not accomplish this, and will instead produce a distorted "sinc"

illumination at the aperture. As an example, Figure A2 shows the aperture amplitude generated by subarray beam No. 7 by the original design and by a uniform-spaced design that keeps the end element of the cylindrical array in the same position.

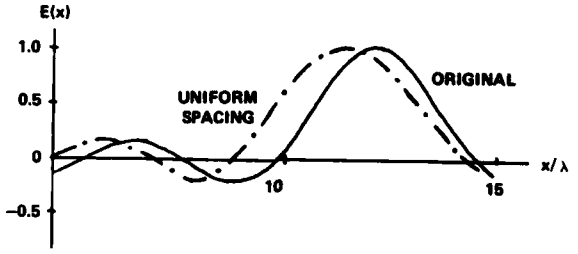

Figure A2. Distorted Aperture Distribution of Subarray Beam No. 7

However, as Figure A3 shows, the total amplitude distribution produced by the 16 weighted subarray beams is not quite so severely distorted. In fact, it yields lower near-in sidelobes (-50 dB vs -35 dB) with no appreciable increase in beam-width, although the far-out sidelobes (near $\theta \pm 90°$) are 10 dB higher than those of the original design.

The distortion in phase is illustrated in Figure A4 for $\alpha_n = n(2°)$ (chosen arbitrarily), and again for a uniform spacing that maintains the original positions of the outside element on each side of the curved face. Under that constraint, the angular spacing between elements is $\xi = 1.67°$. Also shown is the phase given uniform spacing of $\xi = 1.5°$, and the relationship of the three curves shows that there is probably a ξ between 1.5° and 1.7° that yields minimum error with respect to the original design.

Denoting $\Phi(x)$ as the aperture phase created by the original design (assumed continuous and linear):

$$\Phi(x) = \alpha x \tag{A4}$$

we need to find an expression for $\Phi(x, \xi)$, the aperture phase for uniform spacing. In the original case, these points $x_n = d(n - 1/2)$ project straight back onto the curved surface and hence $x_n = F \sin \theta_n$.

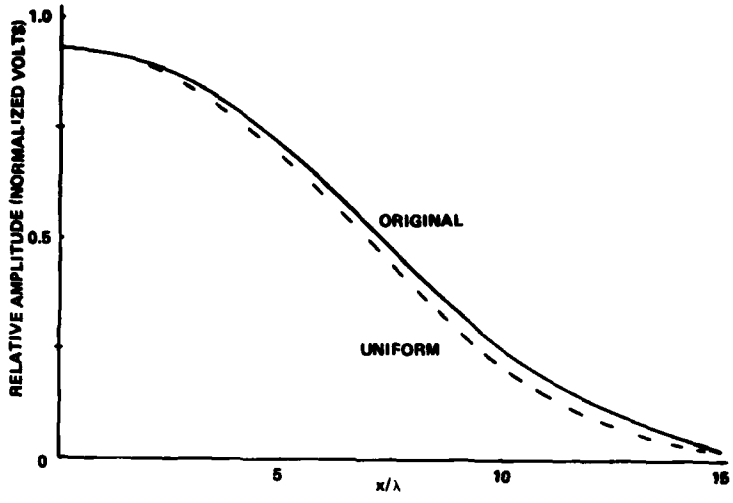

Figure A3. Total Aperture Amplitude Distribution

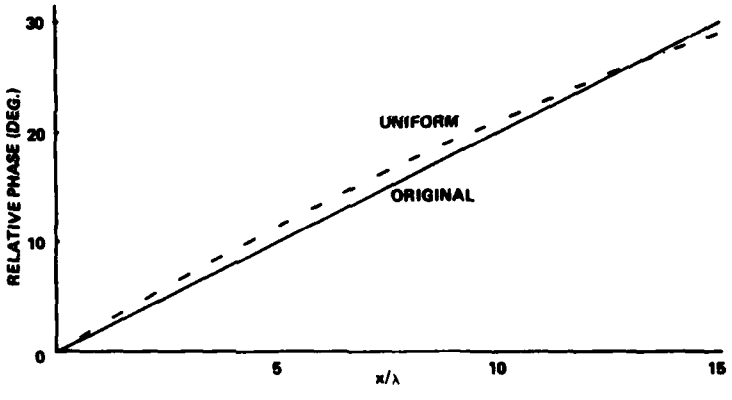

Figure A4. Total Aperture Phase Distribution

In the uniform case, however $\hat{\theta}_n = \xi\,(n - 1/2)$, with ξ a constant and hence

$$\hat{x}_n = F \sin\left[\xi\,(n - \tfrac{1}{2})\right]$$

$$= F \sin\left[\frac{\xi}{d}\, x_n\right]. \qquad \text{(A5)}$$

Therefore,

$$\hat{\Phi}(x, \xi) = \alpha F \sin\left[\frac{\xi x}{d}\right]. \tag{A6}$$

We want to minimize the total squared phase error over the aperture, ϵ_1:

$$\epsilon_1 = \int_{-\ell}^{\ell} \left[\Phi(x) - \hat{\Phi}(x)\right]^2 dx$$

$$= 2\int_{0}^{\ell} \left[\Phi(x) - \hat{\Phi}(x)\right]^2 dx$$

$$\frac{\epsilon_1}{2\alpha^2} = \int_{0}^{\ell} \left[x - F \sin\left(\frac{\xi x}{d}\right)\right]^2 dx \tag{A7}$$

$$= \frac{\ell^3}{3} + \frac{\ell F^2}{2} - \frac{dF^2}{4\xi} \sin\left(\frac{2\xi\ell}{d}\right) - \frac{2d^2F}{\xi^2} \sin(\xi\ell/d)$$

$$+ \frac{2F\ell d}{\xi} \cos(\xi\ell/d).$$

For the parameters $d = 0.5\lambda$, $\ell = 15\lambda$ and $F = 19.44\lambda$, ϵ_1 is minimum at $\xi = 1.57°$. We could also choose to minimize the error in the phase gradient, which is the condition for minimum squint:

$$\epsilon_2 = \int_{-\ell}^{\ell} \left[\frac{d\Phi}{dx} - \frac{d\hat{\Phi}}{dx}\right]^2 dx$$

$$= 2\alpha^2 \int_{0}^{\ell} \left[1 - \frac{\xi F}{d} \cos\left(\frac{\xi x}{d}\right)\right]^2 dx$$

$$\frac{\epsilon_2}{2\alpha^2} = \ell + \frac{\xi^2 F^2 \ell}{2d^2} + \frac{\xi F^2}{4d} \sin\left(\frac{2\xi\ell}{d}\right) - 2F \sin\left(\frac{\xi\ell}{d}\right) \tag{A8}$$

Equation (A8) is minimum at $\xi = 1.58°$.

Because the factor α increases both with scan angle and shift from center frequency so will the errors. Because those errors are small and non-random, they

affect the pattern primarily in the main beam region. As Figure A5 illustrates, the pattern is unaffected at all scan angles at center frequency, and at all frequencies for broadside scan. But at $f = 1.1\, f_o$ and $\theta_o = 55°$ (the extreme design limit of bandwidth and scan angle for this antenna) phase error adds a significant amount of power to the first sidelobe. Figure A6 shows the strength of this sidelobe as a function of ξ, again for $f = 1.1\, f_o$ and $\theta_o = 55°$. This simulation, combined with the results of Eqs. (A7) and (A8) led to the choice of $\xi = 1.55°$ for this antenna. Figure A7 shows the strength in dB of the highest sidelobe vs both scan angle and frequency. The uniform-spaced design's performance thus exceeds the original design's over most of the region of interest (that is, -35 dB peak sidelobe).

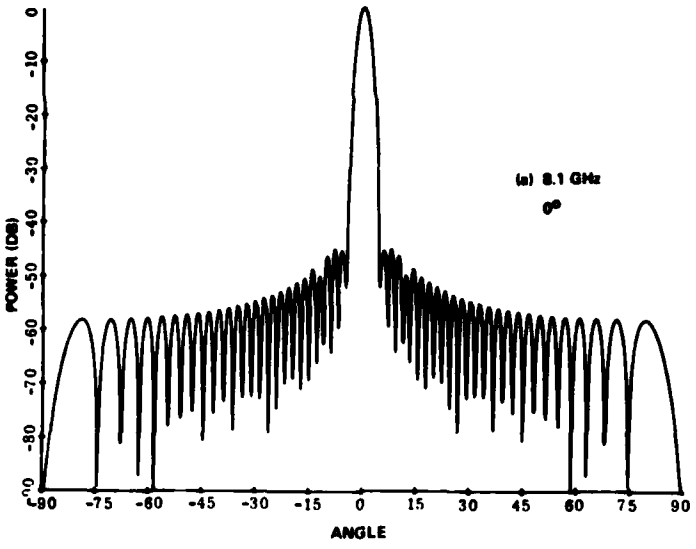

(a)

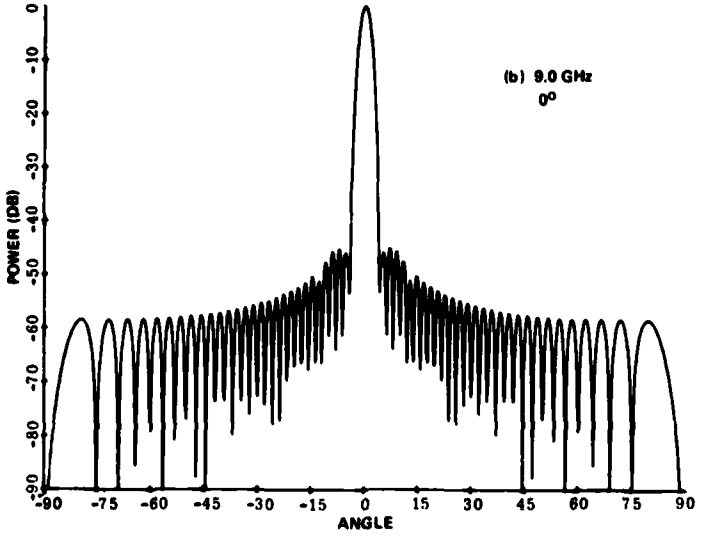

(b)

Figure A5. Theoretical Antenna Patterns

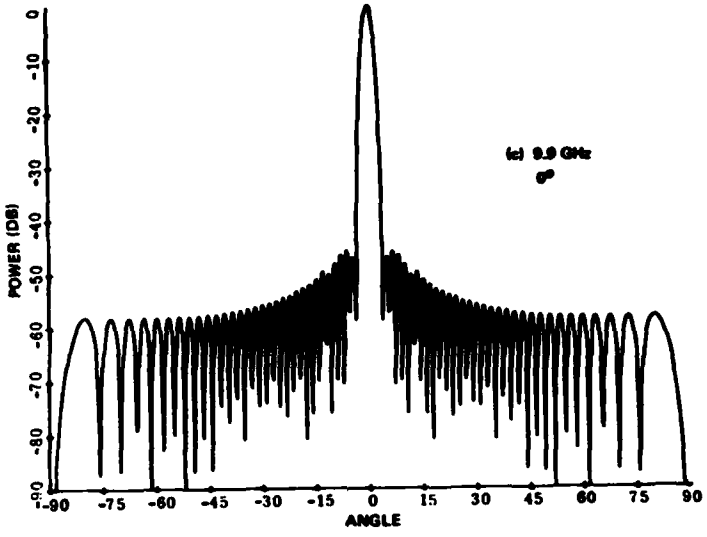

(c)

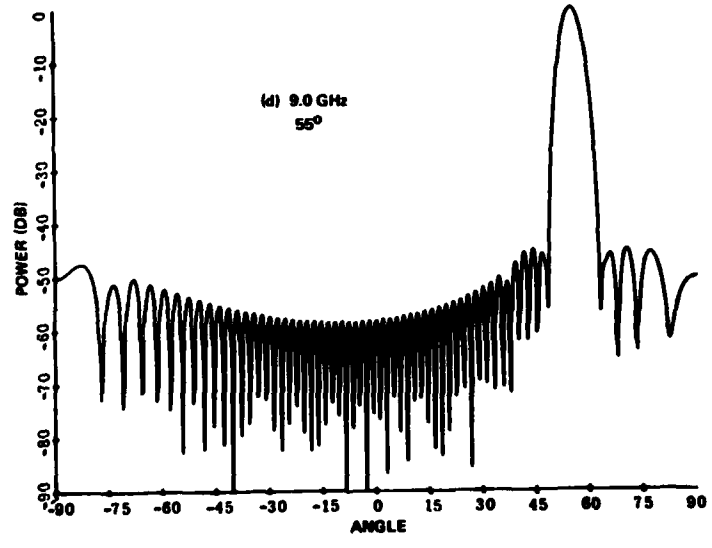

(d)

Figure A5. (Contd)

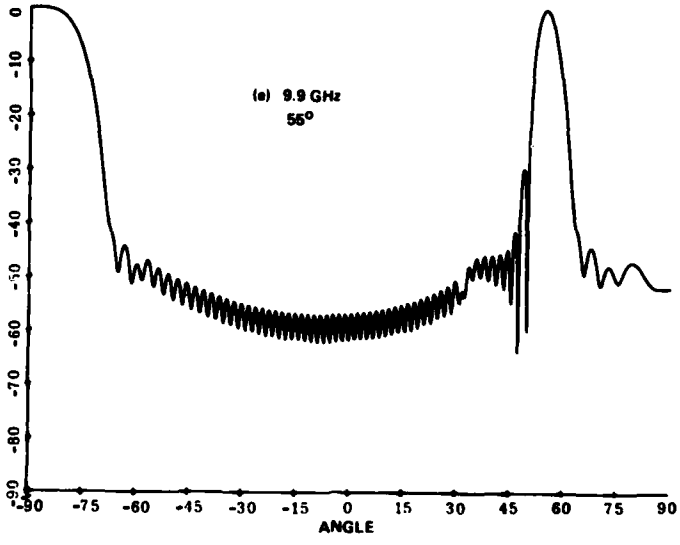

(e)

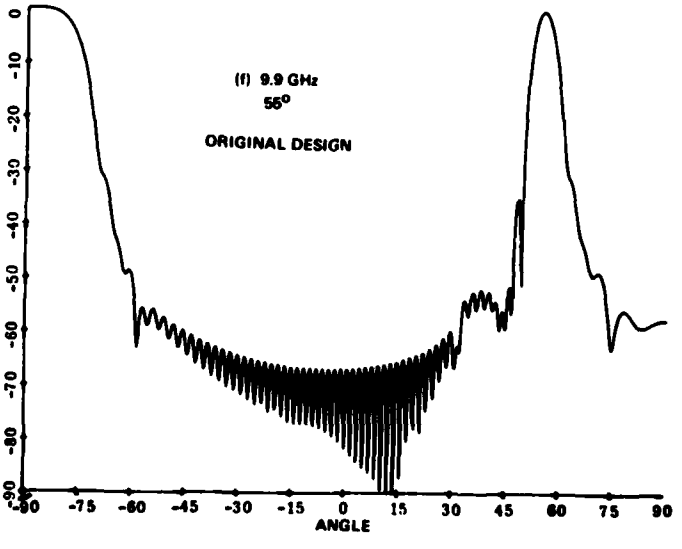

(f)

Figure A5. (Contd)

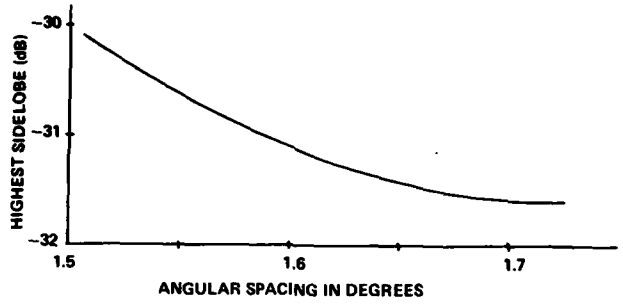

Figure A6. Strength of First Sidelobe vs Probe Spacing

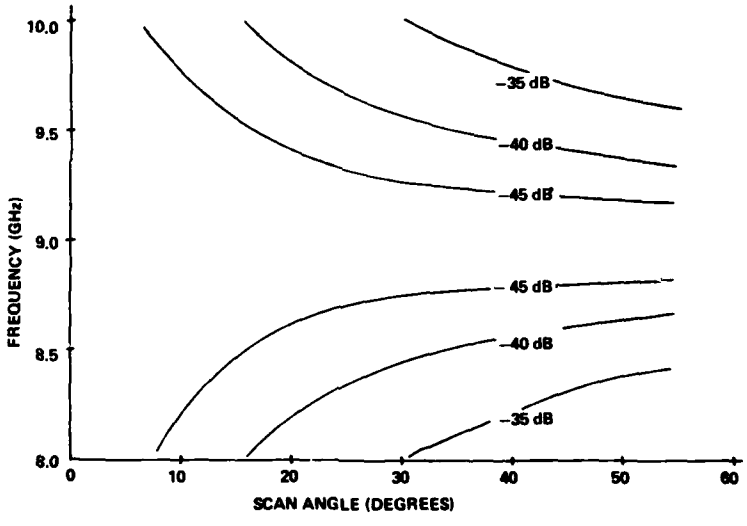

Figure A7. Peak Sidelobe Level vs Scan Angle and Frequency

MISSION
of
Rome Air Development Center

RADC plans and executes research, development, test and selected acquisition programs in support of Command, Control Communications and Intelligence (C^3I) activities. Technical and engineering support within areas of technical competence is provided to ESD Program Offices (POs) and other ESD elements. The principal technical mission areas are communications, electromagnetic guidance and control, surveillance of ground and aerospace objects, intelligence data collection and handling, information system technology, ionospheric propagation, solid state sciences, microwave physics and electronic reliability, maintainability and compatibility.

Printed by
United States Air Force
Hanscom AFB, Mass. 01731

END

FILMED

12-84

DTIC